Editors' Suggestion | Featured in Physics

# Single-Molecule Force Spectroscopy Reveals Cation-$\pi$ Interactions in Aqueous Media Are Highly Affected by Cation Dehydration

Weishuai Di,[1] Kai Xue,[2,3] Jun Cai,[4] Zhenshu Zhu,[5] Zihan Li,[2] Hui Fu,[2] Hai Lei,[5] Wenbing Hu,[4] Chun Tang,[2,*] Wei Wang,[5,6,7,†] and Yi Cao[1,5,6,7,‡]

[1]*Wenzhou Key Laboratory of Biophysics, Wenzhou Institute, University of Chinese Academy of Sciences, Wenzhou, Zhejiang 325000, China*

[2]*Beijing National Laboratory for Molecular Sciences, College of Chemistry and Molecular Engineering, and Peking-Tsinghua Center for Life Sciences, Peking University, Beijing 100871, China*

[3]*School of Physical and Mathematical Science Nanyang Technological University, 21 Nanyang Link, Singapore 637371, Singapore*

[4]*Department of Polymer Science and Engineering, State Key Laboratory of Coordination Chemistry, Collaborative Innovation Center of Chemistry for Life Sciences, School of Chemistry and Chemical Engineering, Nanjing University, 210023 Nanjing, China*

[5]*Collaborative Innovation Center of Advanced Microstructures, National Laboratory of Solid State Microstructure, Department of Physics, Nanjing University, Nanjing 210093, China*

[6]*Institute for Brain Sciences, Nanjing University, Nanjing 210093, China*

[7]*Chemistry and Biomedicine Innovation Center, Nanjing University, Nanjing 210093, China*

(Received 2 August 2022; accepted 24 January 2023; published 17 March 2023)

Cation-$\pi$ interactions underlie many important processes in biology and materials science. However, experimental investigations of cation-$\pi$ interactions in aqueous media remain challenging. Here, we studied the cation-$\pi$ binding strength and mechanism by pulling two hydrophobic polymers with distinct cation binding properties, i.e., poly-pentafluorostyrene and polystyrene, in aqueous media using single-molecule force spectroscopy and nuclear magnetic resonance measurement. We found that the interaction strengths linearly depend on the cation concentrations, following the order of $Li^+ < NH_4^+ < Na^+ < K^+$. The binding energies are 0.03–0.23 kJ mol$^{-1}$ M$^{-1}$. This order is distinct from the strength of cation-$\pi$ interactions in gas phase and may be caused by the different dehydration ability of the cations. Taken together, our method provides a unique perspective to investigate cation-$\pi$ interactions under physiologically relevant conditions.

DOI: 10.1103/PhysRevLett.130.118101

Cation-$\pi$ interaction, arising from an attractive force between a $\pi$ electron cloud and a positive charge, is ubiquitously found in nature [1–4]. Dougherty *et al.* pointed out that electrostatic force is vital to cation-$\pi$ interaction [5,6]. They proposed an electrostatic force model that can interpret the binding strength order, $K^+ \approx NH_4^+ < Na^+ < Li^+$, in the gas phase [7,8]. Later studies revealed that polarization force, induction force, and dispersion force are also important to cation-$\pi$ interaction in different cation and $\pi$ systems [9–12].

Cation-$\pi$ interaction plays important roles in many biochemical processes, including protein folding, molecular recognition, ion channels, and catalysis [13–17]. Because of the interplay between the hydration and dehydration of ions, cation-$\pi$ interaction is more complicated in the aqueous environment than in the gas phase. Previous studies pointed out that $K^+$ preferred binding with benzene more than hydration in water [8,18]. Unconventional stoichiometries of Na-Cl crystals on graphene surfaces indicated that $Na^+$ was partially dehydrated to form $Na^+$-$\pi$ interactions [19]. Previous simulation results suggested that the binding energetics of the cation-$\pi$ complex are influenced by the solvent effect and spatial restriction [15,20,21]. However, it is challenging to experimentally study the dehydration and solvent effect of cation-$\pi$ binding at the nanoscale.

Here, we reported a single-molecule force spectroscopy (SMFS) assay [22–32] based on atomic force microscopy (AFM) for investigating the cation-$\pi$ interactions in aqueous media. In our previous work [33], we found stretching hydrophobic polymers [i.e., polystyrene (PS)] in aqueous media yielded characteristic plateau-shape force-extension curves, and the plateau forces were correlated with the solvation free energy. Fluorine-substituted polymers [i.e., poly-pentafluorostyrene (PPFS)] showed the same plateau forces as PS [34]. In this Letter, we explored how cations affect the plateau forces of two polymers. We found the plateau forces of PPFS can be described using a physical model only considering the hydrophobic effects. However, the plateau forces of PS cannot be described using the same

 

model. We propose that such a discrepancy is due to the cation-$\pi$ interactions. By extending the model to include the cation-$\pi$ interactions, we can adequately describe the experimental data. More surprisingly, we found the strength of cation-$\pi$ interactions followed the order of $Li^+ < NH_4^+ < Na^+ < K^+$, distinct from that in the gas phase. NMR experiments suggested that hydrated $Li^+$ could enter collapsed PS nanospheres directly upon cation-$\pi$ interactions, while $Na^+$ dehydrated before entering PS. Our results highlighted the importance of the hydration or dehydration effect on the cation-$\pi$ interactions in aqueous media.

We synthesized PPFS and PS with additional functional groups on both ends (Fig. S1 in the Supplemental Material [35]), thus, to facilitate covalent linkage with the glass substrate and the cantilever tip for AFM experiments. In PPFS, the fluorine-substituted benzene rings are electronically deficient, and therefore, cannot form cation-$\pi$ interactions. In contrast, the benzene rings in PS are good $\pi$ donors and can form cation-$\pi$ interactions. To confirm the cation-$\pi$ interactions of PS with cations, we mixed PS with various salts and determined the glass transition temperature ($T_g$) using differential scanning calorimetry [39]. We observed that $T_g$ of PS was lowered when mixing with various cations, suggesting that cation-$\pi$ binding makes the PS chains more mobile in a condensed phase (Fig. S2 in the Supplemental Material [35]).

We conducted the SMFS experiments in water [Fig. 1(a) and, in the Supplemental Material, Fig. S1 [35] ]. Owing to hydrophobicity, PPFS and PS polymer chains collapse into nanospheres [40,44–46], as confirmed by AFM imaging with heights of 3–8 nm (Fig. S3 in the Supplemental Material [35]). When the AFM tip modified with maleimide groups was extended to the substrate, the maleimide reacted with the thiol group on the other end of the polymers. Subsequently, the AFM cantilever was retracted to unfold the collapsed polymer nanospheres. The representative force-extension curves are shown in Fig. 1(b). The beginning part of that often shows a bump due to the electrostatic interactions between the cantilever tip and the substrate. After that, the curves show a long force plateau around 110 pN, corresponding to unfolding the polymer nanosphere [inset in Fig. 1(b)]. The constant force of the plateaus indicated the unfolding process is reversible [33]. After a complete unfolding of the polymer nanosphere, the force gradually rose up in a fashion that can be described with the wormlike chain (WLC) model [47,48] of polymer elasticity, until the rupture of the polymer. The persistence length of PPFS and PS is $0.23 \pm 0.04$ nm and $0.25 \pm 0.04$ nm, respectively (Fig. S4 in the Supplemental Material [35]). In contrast, the force-extension curves in toluene did not show any force plateaus because the polymers were fully dissolved and adopted random coil conformations in good solvent (Fig. S5 in the Supplemental Material [35]). The force-extension curves normalized by

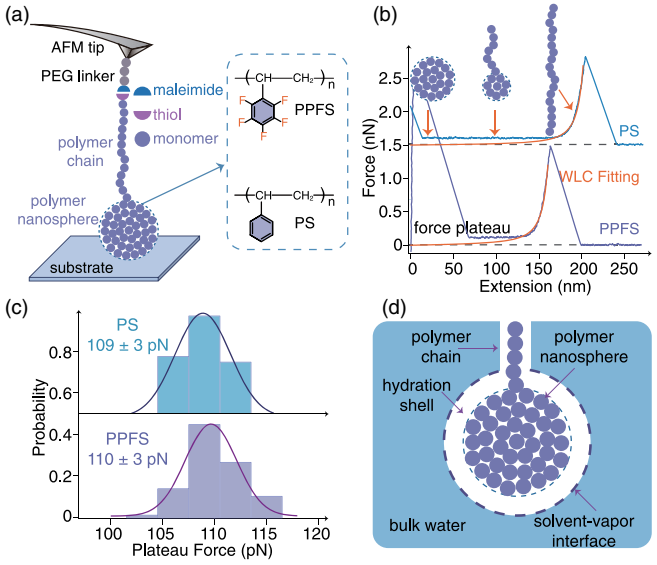


FIG. 1. Pulling collapsed polymer nanospheres in water using the SMFS method. (a) Illustration of the experimental design. Inset is polymer structures. (b) Typical force-extension curves for PPFS and PS. WLC fittings to the elastic stretching part are shown in orange. Dashed line is the base line. Upper inset illustrates the whole unfolding process of the nanosphere. (c) The histogram of plateau force for PPFS and PS collected in one experiment. (d) Illustration of the hydration shell theory.

the contour length in both solvents are shown in Fig. S6 in the Supplemental Material [35]. The elastic stretching parts overlap with each other, indicating that the fully unfolded polymers behave the same in water as that in toluene.

Figure 1(c) shows the histogram of plateau forces for PPFS and PS collected using the same cantilever with minimal cantilever calibration errors. The final plateau forces (the average of averaged value for many experiments, details in Sec. VI of the Supplemental Material [35]) for PPFS ($108 \pm 2$ pN) and PS ($107 \pm 3$ pN) in water are similar, although they are of different chemical properties. This observation agrees with the hydration shell theory [46,49–51]. According to that, the outer surface of the polymer nanosphere and the inner surface of bulk water are separated by a vapor interface [Fig. 1(d)]. In the unfolding process, the polymer chain penetrates the hydration shell and then enters the bulk water. Owing to such vapor interface, the plateau forces depend on the surface tension of water.

To study the cation-$\pi$ interaction, we performed the SMFS experiments in four salt solutions (LiCl, NaCl, KCl, and $NH_4Cl$). Both PPFS and PS showed the nanosphere structures with heights of 3–8 nm under these conditions as revealed by AFM imaging (Figs. S7 and S8 in the Supplemental Material [35]). Note that adding cations to the system not only introduced the cation-$\pi$ interaction but also changed the surface tension of water. Therefore, PPFS served as a reference polymer to estimate the effect of salt concentrations on the hydrophobic interactions. The data

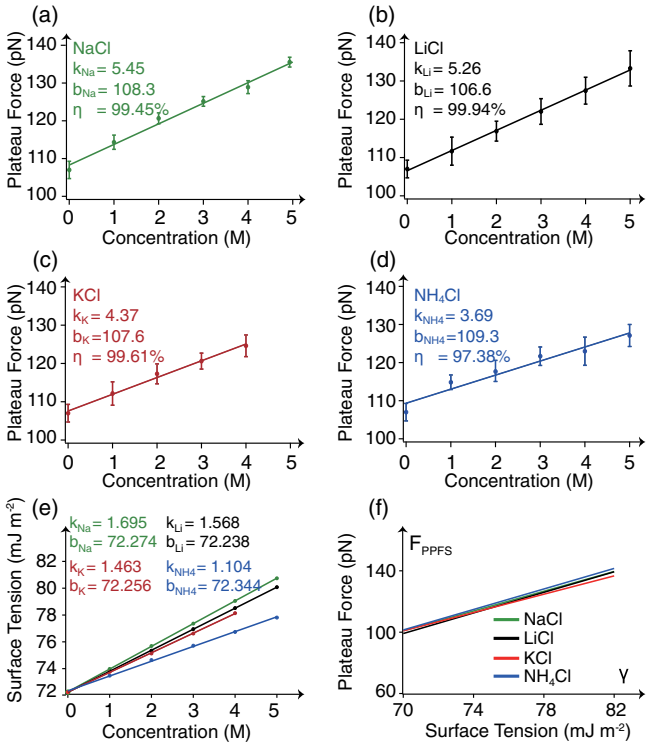


FIG. 2. The data analysis of plateau forces for pulling PPFS nanospheres in salt solutions. (a), (b), (c), and (d) are plateau forces in the NaCl, LiCl, KCl, and $NH_4Cl$ solution, respectively. The error bars represent the standard deviation. The lines are linear fittings to the data. The slope ($k$), intercept ($b$), and linear correlation coefficient ($\eta$) are listed in the figure, respectively. Here, the unit M denotes mol/kg water and similarly hereinafter. (e) The surface tension of the salt solution at different concentrations. The line is the linear fitting to the data with slope ($k$) and intercept ($b$). (f) Four independent lines of Eq. (3) based on the data from Figs. 2(a)–2(e).

points are normalized by the averaged plateau forces collected in water to minimize the calibration errors (Sec. VI of the Supplemental Material [35]). We found the plateau forces of PPFS ($F_{PPFS}$) increased linearly with the salt concentrations $C$ [(Figs. 2(a)–2(d)], namely,

$$F_{PPFS} = k_{PPFS}C + F_0. \quad (1)$$

Here, the slope $k_{PPFS}$ manifests how the plateau forces depend on the salt concentrations, and $F_0$ is the plateau force in water. The slopes in Figs. 2(a)–2(d) follow the order of $NH_4^+ < K^+ < Li^+ < Na^+$.

As PPFS cannot form cation-$\pi$ interactions, we hypothesized that its force plateaus are solely influenced by the surface tension of the salt solutions. We adapted the surface tension of four types of solutions from Ref. [42] as shown in Fig. 2(e). The surface tension linearly depends on the salt concentrations. Hence,

$$\gamma = k_\gamma C + \gamma_0 \quad (2)$$

in which $k_\gamma$ is the dependency of surface tension on the concentration $C$, and $\gamma_0$ is the surface tension of water.

According to Eqs. (1) and (2), we find a linear relationship between the plateau forces and surface tension, namely,

$$F_{PPFS} = k\gamma + \beta. \quad (3)$$

Here, the slope, $k = k_{PPFS}/k_\gamma$, and the intercept, $\beta = F_0 - k\gamma_0$, can be calculated from the data in Fig. 2. Dimensional analysis implies $k$ is with the unit of length. Pulling a polymer to aqueous media can be understood as a process to create a new water-polymer interface against surface tension. Based on Eq. (3), $k$ is physically correlated with the perimeter of the cross section of the polymer chain as illustrated in Fig. 1(d) (details in Sec. VIII of the Supplemental Material [35]).

By plotting Eq. (3) obtained from the four different salt solutions, we found the four curves are almost identical within errors [Fig. 2(f)]. These findings indicate that the plateau forces are unrelated to the type of the salt if the surface tension of the salt solution is same.

Next, we unfolded PS nanospheres using SMFS in salt solutions. The plateau forces are summarized in Figs. 3(a)–3(d) and also increase linearly with the salt concentrations

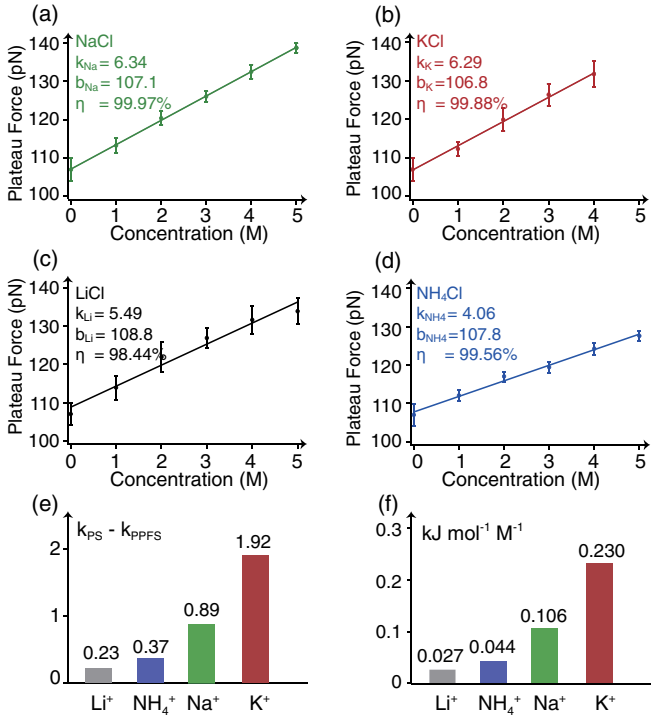


FIG. 3. Determining cation-$\pi$ binding strengths from SMFS data. (a), (b), (c), and (d) are concentration-dependent plateau forces for the NaCl, LiCl, KCl, and $NH_4Cl$ solutions, respectively. (e) The difference between the slopes of salt concentration dependent plateau forces of PS and PPFS. (f) The cation-$\pi$ binding energy averaged by the number of monomers and cation concentrations.

(Sec. VIII of the Supplemental Material [35]). The relationship between plateau forces of PS ($F_{PS}$) and salt concentrations can be described as

$$F_{PS} = k_{PS}C + F_0 \tag{4}$$

where $k_{PS}$ is the slope of PS in various salt solutions and $F_0$ is the plateau force of PS in water, which is the same as that of PPFS. The slopes that measure how the plateau forces depend on the salt concentrations follow a different order compared with PPFS. The new order is $NH_4^+ < Li^+ < K^+ < Na^+$.

Compared with PPFS, which cannot bind with cations in solutions, PS can bind with cations in solutions through cation-$\pi$ interactions. The unfolding process in salt solutions involves the rupture of the cation-$\pi$ interactions that bridge two phenyl groups from different positions in the folded PS nanosphere. That means that one cation binds with two phenyl groups simultaneously [13] (Sec. IX of the Supplemental Material [35]). Therefore, the plateau forces of PS are expected to be larger than that of PPFS (Note that the hanging cation-$\pi$ bindings on the PS chain do not contribute to the plateau force). Indeed, the slopes for PS in all types of salt solutions are larger than that for PPFS. Since the increase of force implies the presence of cation-$\pi$ interactions, we hypothesized that the distinct changes of the slopes are associated with the different cation-$\pi$ interaction strengths.

Considering that the energy ($E_{PS}$) stored in the PS nanosphere is contributed by hydrophobic interactions ($E_{PS\text{-hydrophobic}}$) and cation-$\pi$ interactions ($E_{cation\text{-}\pi}$)

$$E_{PS} = E_{PS\text{-hydrophobic}} + E_{cation\text{-}\pi}, \tag{5}$$

while $E_{PPFS}$ is contributed by hydrophobic interactions:

$$E_{PPFS} = E_{PPFS\text{-hydrophobic}}. \tag{6}$$

Based on the analysis of Eqs. (1)–(4), we supposed the hydrophobic interactions for the PS and PPFS were the same, $E_{PS\text{-hydrophobic}} = E_{PPFS\text{-hydrophobic}}$. Therefore,

$$E_{cation\text{-}\pi} = E_{PS} - E_{PPFS}. \tag{7}$$

This can be reduced to a "force" form (Sec. X of the Supplemental Material [35])

$$F_{cation\text{-}\pi} = (k_{PS} - k_{PPFS})C. \tag{8}$$

Interestingly, we find the cation $\pi$, behaving as a force, constitutes a part of the plateau force. The difference of the slopes of PS and PPFS is a measure of relative strength of the cation-$\pi$ interactions [Fig. 3(e)].

The strength of cation-$\pi$ interactions was estimated based on ($k_{PS} - k_{PPFS}$) (Sec. X of the Supplemental Material [35]). The binding energy is 0.03–0.23 kJ mol$^{-1}$ M$^{-1}$ [Fig. 3(f)], smaller than that predicted by the point-to-point binding model from simulations [21]. This is reasonable because our calculation considers the environmental concentration of the cations, the reduced number of benzene rings due to the steric hindrance, and the weakened cation-$\pi$ interactions by a surrounding dielectric medium in our system [52].

We found the cation-$\pi$ interactions between four cations and PS follows the order $Li^+ < NH_4^+ < Na^+ < K^+$. It is different from the order $NH_4^+ \approx K^+ < Na^+ < Li^+$ in the gas phase that was predicted by the electrostatic model [7,8], and is also different from Zeng's results, $Li^+ < Na^+ < K^+ < NH_4^+$ [53], measured by surface forces apparatus using competitive binding in aqueous solution. The discrepancy may be due to the hydration effect of the metal ions. In the gas phase, all metal ions are dehydrated. In Zeng's experiments, all metal ions are water bound. However, in our case, the PS is hydrophobic, and whether cations carry water molecules into the PS nanospheres depends on the interplay of the dehydration energy and the cation-$\pi$ interaction. The binding of cation ($M^+$) with the $\pi$ system in PS can be described as follows: For relatively weak hydration,

$$M^+(H_2O)_n + \pi \rightleftarrows [M^+ - \pi] + n(H_2O). \tag{9}$$

Or for relatively strong hydration,

$$M^+(H_2O)_n + \pi \rightleftarrows [M^+(H_2O)_n - \pi]. \tag{10}$$

The $K^+$ shows stronger affinity with benzene than with water [54]; thus the hydrated $K^+$ dehydrates to enter the PS nanosphere [Fig. 4(a), Eq. (9)]. For $Na^+$, the $Na^+$-benzene binding strength is stronger than $K^+$-benzene in the gas phase, but the hydration energy of $Na^+$ is 1.3 times of that of $K^+$ [55]. Thus, the net energy change for $Na^+$ is smaller than $K^+$. The hydration energy of $Li^+$ is the largest among these cations. Therefore, $Li^+$ does not dehydrate but carries bound water to PS [Eq. (10)]. Similarly, $NH_4^+$ also carries bound water to PS. The mechanism is schematically shown in Fig. 4(a).

To further evaluate this mechanism, we used solid-state NMR experiments to investigate the properties of PS spheres mixed with LiCl and NaCl solutions. The proton 1D spectrum of PS + LiCl shows an additional sharp peak that does not appear in PS and PS + NaCl samples [Fig. 4(b)]. This peak is close to the signal from crystalline water, indicating that LiCl is accompanied by water due to the strong hydration ability. Next, we performed the solid-state NMR HETCOR experiment with an additive T2 filter to filter out proton signals from PS and preserved only crystalline water signals in the beginning of the pulse sequence. Furthermore, we used spin diffusion to estimate

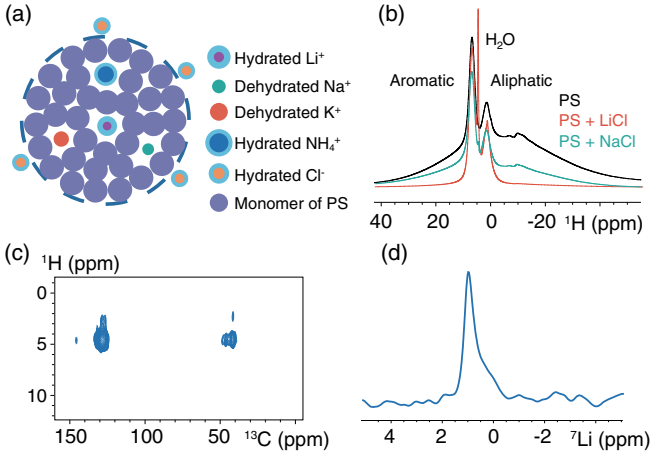


FIG. 4. NMR studies of the interaction between hydrated $Li^+$ and PS. (a) A schematic illustration of dehydrated $K^+$, $Na^+$ and hydrated $Li^+$, $NH_4^+$ entering the PS nanosphere. (b) The proton 1D spectrum for PS, PS + LiCl, and PS + NaCl. (c) Spectrum of a 100-μs H-H spin diffusion encoded HETCOR experiment. Measurement was performed at a 20 kHz magic angle spinning at 600 MHz magnetic field. (d) Spectrum of $^1$H-$^7$Li CP (contact time of 400 μs) at 20 kHz magic angle spinning.

the distance between crystalline water and PS aromatic protons. Pulse sequences are shown in Fig. S10 of the Supplemental Material [35], and the $^1$H-$^{13}$C correlation spectrum is shown in Fig. 4(c). Since 0.05–0.1 ms of spin diffusion time is enough to afford correlated spectra between crystalline water and PS, we estimated the distance between water and PS to be 0.35–0.5 nm [56]. We also performed a T2-filtered $^1$H-$^7$Li cross polarization (CP) experiment using the pulse sequence shown in Fig. S10 of the Supplemental Material [35]. With only 0.4 ms of CP contact time, we observed the signal transfer from crystalline water to $Li^+$ [Fig. 4(d)]. Thus, water is always closer to $Li^+$ than to the benzene ring—the hydrated $Li^+$ enters the PS nanosphere, different from $Na^+$. As the water molecules screen the charge of $Li^+$ and increase the distance to benzene rings, the $Li^+$ shows the weakest binding strength to benzene among the four cations.

In summary, we developed an AFM-based SMFS method to determine the cation-$\pi$ binding mechanism at the nanoscale in aqueous solution. Using a polymer that cannot bind with cations as the reference polymer, we can infer the strength of cation-$\pi$ interactions from their different cation-concentration-dependent unfolding plateau forces. Furthermore, based on single-molecule data, we found the cation-$\pi$ interaction strength is linearly proportional to cation concentrations, which is distinct from the specific interactions that saturate at high ligand concentrations. The cation-$\pi$ interaction strength follows the order of $Li^+ < NH_4^+ < Na^+ < K^+$. This order is distinct from the strength of cation-$\pi$ interactions in the gas phase. Solid-state NMR measurements suggested that a competition between the cation-$\pi$ binding and the cation-water (hydrated cation) interactions determines whether the cations enter the hydrophobic PS nanospheres alone or with bound water molecules. $K^+$ and $Na^+$ prefer to be dehydrated prior to entering the PS nanosphere and forming cation-$\pi$ interactions. Energetically, $NH_4^+$ and $Li^+$ tend to maintain their hydrated states. To summarize, our studies provide a new insight of the cation-$\pi$ interactions in aqueous environments and at hydrophilic-hydrophobic interfaces.

This research is supported mainly by the National Science Fund for Distinguished Young Scholars (Grant No. T2225016), the National Key R&D Program of China (Grant No. 2020YFA0908100), and the National Natural Science Foundation of China (Grant No. 21774057).

*Corresponding author.
tang_chun@pku.edu.cn
†Corresponding author.
wangwei@nju.edu.cn
‡Corresponding author.
caoyi@nju.edu.cn

[1] A. S. Mahadevi and G. N. Sastry, Cation-$\pi$ interaction: Its role and relevance in chemistry, biology, and material science, Chem. Rev. **113**, 2100 (2013).
[2] G. Shi, Y. Dang, T. Pan, X. Liu, H. Liu, S. Li, L. Zhang, H. Zhao, S. Li, J. Han, R. Tai, Y. Zhu, J. Li, Q. Ji, R. A. Mole, D. Yu, and H. Fang, Unexpectedly Enhanced Solubility of Aromatic Amino Acids and Peptides in an Aqueous Solution of Divalent Transition-Metal Cations, Phys. Rev. Lett. **117**, 238102 (2016).
[3] S. Hong, Y. Wang, S. Y. Park, and H. Lee, Progressive fuzzy cation-$\pi$ assembly of biological catecholamines, Sci. Adv. **4**, eaat7457 (2018).
[4] P. Zheng, L. Xiang, J. Chang, Q. Lin, L. Xie, T. Lan, J. Liu, Z. Gong, T. Tang, L. Shuai, X. Luo, N. Chen, and H. Zeng, Nanomechanics of lignin-cellulase interactions in aqueous solutions, Biomacromolecules **22**, 2033 (2021).
[5] S. Mecozzi, A. P. West, and D. A. Dougherty, Cation-$\pi$ interactions in simple aromatics: Electrostatics provide a predictive tool, J. Am. Chem. Soc. **118**, 2307 (1996).
[6] S. Mecozzi, A. P. West, and D. A. Dougherty, Cation-pi interactions in aromatics of biological and medicinal interest: electrostatic potential surfaces as a useful qualitative guide, Proc. Natl. Acad. Sci. U.S.A. **93**, 10566 (1996).
[7] J. C. Ma and D. A. Dougherty, The cation-$\pi$ interaction, Chem. Rev. **97**, 1303 (1997).
[8] D. A. Dougherty, The cation-$\pi$ interaction, Acc. Chem. Res. **46**, 885 (2013).
[9] E. Cubero, F. J. Luque, and M. Orozco, Is polarization important in cation-$\pi$ interactions?, Proc. Natl. Acad. Sci. U.S.A. **95**, 5976 (1998).
[10] S. Tsuzuki, M. Yoshida, T. Uchimaru, and M. Mikami, The origin of the cation/$\pi$ interaction: The significant importance of the induction in $Li^+$ and $Na^+$ complexes, J. Phys. Chem. A **105**, 769 (2001).

[11] D. Kim, S. Hu, P. Tarakeshwar, K. S. Kim, and J. M. Lisy, Cation-$\pi$ interactions: A theoretical investigation of the interaction of metallic and organic cations with alkenes, arenes, and heteroarenes, J. Phys. Chem. A **107**, 1228 (2003).

[12] I. Soteras, M. Orozco, and F. J. Luque, Induction effects in metal cation–benzene complexes, Phys. Chem. Chem. Phys. **10**, 2616 (2008).

[13] R. A. Kumpf and D. A. Dougherty, A mechanism for ion selectivity in potassium channels: Computational studies of cation-$\pi$ interactions, Science **261**, 1708 (1993).

[14] J. D. Schmitt, C. G. V. Sharples, and W. S. Caldwell, Molecular recognition in nicotinic acetylcholine receptors: The importance of $\pi$-cation interactions, J. Med. Chem. **42**, 3066 (1999).

[15] P. B. Crowley and A. Golovin, Cation-$\pi$ interactions in protein–protein interfaces, Proteins **59**, 231 (2005).

[16] C. H. Chiang and J. C. Horng, Cation-$\pi$ interaction induced folding of AAB-type collagen heterotrimers, J. Phys. Chem. B **120**, 1205 (2016).

[17] C. R. Kennedy, S. Lin, and E. N. Jacobsen, The cation-$\pi$ interaction in small-molecule catalysis, Angew. Chem., Int. Ed. **55**, 12596 (2016).

[18] O. M. Cabarcos, C. J. Weinheimer, and J. M. Lisy, Competitive solvation of $K^+$ by benzene and water: Cation-$\pi$ interactions and $\pi$-hydrogen bonds, J. Chem. Phys. **108**, 5151 (1998).

[19] G. Shi, L. Chen, Y. Yang, D. Li, Z. Qian, S. Liang, L. Yan, L. H. Li, M. Wu, and H. Fang, Two-dimensional Na-Cl crystals of unconventional stoichiometries on graphene surface from dilute solution at ambient conditions, Nat. Chem. **10**, 776 (2018).

[20] S. Tsuzuki, M. Mikami, and S. Yamada, Origin of attraction, magnitude, and directionality of interactions in benzene complexes with pyridinium cations, J. Am. Chem. Soc. **129**, 8656 (2007).

[21] M. S. Marshall, R. P. Steele, K. S. Thanthiriwatte, and C. D. Sherrill, Potential energy curves for cation-$\pi$ interactions: Off-axis configurations are also attractive, J. Phys. Chem. A **113**, 13628 (2009).

[22] W. Cai, D. Xu, L. Qian, J. Wei, C. Xiao, L. Qian, Z. Y. Lu, and S. Cui, Force-induced transition of $\pi$-$\pi$ stacking in a single polystyrene chain, J. Am. Chem. Soc. **141**, 9500 (2019).

[23] Y. Tian, X. Cao, X. Li, H. Zhang, C. L. Sun, Y. Xu, W. Weng, W. Zhang, and R. Boulatov, A polymer with mechanochemically active hidden length, J. Phys. Chem. A **142**, 18687 (2020).

[24] Y. Bao, X. Huang, J. Xu, and S. Cui, Effect of intramolecular hydrogen bonds on the single-chain elasticity of poly (vinyl alcohol): Evidencing the synergistic enhancement effect at the single-molecule level, Macromolecules **54**, 7314 (2021).

[25] J. Li, G. Chen, Y. Guo, H. Wang, and H. Li, Single molecule force spectroscopy reveals the context dependent folding pathway of the C-terminal fragment of Top7, Chem. Sci. **12**, 2876 (2021).

[26] R. Yao, X. Li, N. Xiao, W. Weng, and W. Zhang, Single-molecule observation of mechanical isomerization of spirothiopyran and subsequent Click addition, Nano Res. **14**, 2654 (2021).

[27] H. Yu, D. R. Jacobson, H. Luo, and T. T. Perkins, Quantifying the Native Energetics Stabilizing Bacteriorhodopsin by Single-Molecule Force Spectroscopy, Phys. Rev. Lett. **125**, 068102 (2020).

[28] Z. Liu, H. Liu, A. M. Vera, R. C. Bernardi, P. Tinnefeld, and M. A. Nash, High force catch bond mechanism of bacterial adhesion in the human gut, Nat. Commun. **11**, 4321 (2020).

[29] A. Kolberg, C. Wenzel, K. Hackenstrass, R. Schwarzl, C. Rttiger, T. Hugel, M. Gallei, R. R. Netz, and B. N. Balzer, Opposing temperature dependence of the stretching response of single PEG and PNiPAM polymers, J. Am. Chem. Soc. **141**, 11603 (2019).

[30] D. T. Edwards, M. A. LeBlanc, and T. T. Perkins, Modulation of a protein-folding landscape revealed by AFM-based force spectroscopy notwithstanding instrumental limitations, Proc. Natl. Acad. Sci. U.S.A. **118**, e2015728118 (2021).

[31] P. Lopez-Garcia, A. D. de Araujo, A. E. Bergues-Pupo, I. Tunn, D. P. Fairlie, and K. G. Blank, Fortified coiled coils: Enhancing mechanical stability with lactam or metal staples, Angew. Chem., Int. Ed. **60**, 232 (2021).

[32] M. Yu, S. Le, S. Barnett, Z. Guo, X. Zhong, P. Kanchanawong, and J. Yan, Implementing Optogenetic Modulation in Mechanotransduction, Phys. Rev. X **10**, 021001 (2020).

[33] W. Di, X. Gao, W. Huang, Y. Sun, H. Lei, Y. Liu, W. Li, Y. Li, X. Wang, M. Qin, Z. Zhu, Y. Cao, and W. Wang, Direct Measurement of Length Scale Dependence of the Hydrophobic Free Energy of a Single Collapsed Polymer Nanosphere, Phys. Rev. Lett. **122**, 047801 (2019).

[34] W. Di, X. Wang, Y. Zhou, Y. Mei, W.Wang, and Y. Cao, Fluorination increases hydrophobicity at the macroscopic level but not at the microscopic level, Chin. Phys. Lett. **39**, 038701 (2022).

[35] See Supplemental Material at http://link.aps.org/supplemental/10.1103/PhysRevLett.130.118101 for additional experimental details, methods and derivations, which includes Refs. [13,33,34,36–43].

[36] M. Lansalot, T. P. Davis, and J. P. A. Heuts, RAFT miniemulsion polymerization: Influence of the structure of the RAFT agent, Macromolecules **35**, 7582 (2002).

[37] K. M. Gattás-Asfura and C. L. Stabler, Chemoselective cross-linking and functionalization of alginate via staudinger ligation, Biomacromolecules **10**, 3122 (2009).

[38] M. Köhn and R. Breinbauer, The staudinger ligation-a gift to chemical biology, Angew. Chem., Int. Ed. **43**, 3106 (2004).

[39] G. Chang, L. Yang, J. Yang, M. P. Stoykovich, X. Deng, J. Cui, and D. Wang, High-performance pH-switchable supramolecular thermosets via cation-$\pi$ interactions, Adv. Mater. **30**, 1704234 (2018).

[40] I. T. S. Li and G. C. Walker, Interfacial free energy governs single polystyrene chain collapse in water and aqueous solutions, J. Am. Chem. Soc. **132**, 6530 (2010).

[41] R. I. Slavchov and J. K. Novev, Surface tension of concentrated electrolyte solutions, J. Colloid Interface Sci. **387**, 234 (2012).

[42] N. L. Jarvis and M. A. Scheiman, Surface potentials of aqueous electrolyte solutions, J. Chem. Phys. **72**, 74 (1968).
[43] P. K. Weissenborn and R. J. Pugh, Surface tension of aqueous solutions of electrolytes: Relationship with ion hydration, oxygen solubility, and bubble coalescence, J. Colloid Interface Sci. **184**, 550 (1996).
[44] I. T. S. Li and G. C. Walker, Signature of hydrophobic hydration in a single polymer, Proc. Natl. Acad. Sci. U.S.A. **108**, 16527 (2011).
[45] P. R. ten Wolde and D. Chandler, Drying-induced hydrophobic polymer collapse, Proc. Natl. Acad. Sci. U.S.A. **99**, 6539 (2002).
[46] D. Chandler, Interfaces and the driving force of hydrophobic assembly, Nature (London) **437**, 640 (2005).
[47] J. F. Marko and E. D. Siggia, Stretching DNA, Macromolecules **28**, 8759 (1995).
[48] Y. Bao, Z. Luo, and S. Cui, Environment-dependent single-chain mechanics of synthetic polymers and biomacromolecules by atomic force microscopy-based single-molecule force spectroscopy and the implications for advanced polymer materials, Chem. Soc. Rev. **49**, 2799 (2020).
[49] J. Mittal and G. Hummer, Static and dynamic correlations in water at hydrophobic interfaces, Proc. Natl. Acad. Sci. U.S.A. **105**, 20130 (2008).
[50] A.Wallqvist, E. Gallicchio, and R. M. Levy, A model for studying drying at hydrophobic interfaces: Structural and thermodynamic properties, J. Phys. Chem. B **105**, 6745 (2001).
[51] D. M. Huang and D. Chandler, The hydrophobic effect and the influence of solute-solvent attractions, J. Phys. Chem. B **106**, 2047 (2002).
[52] K. Kumar, S. M. Woo, T. Siu, W. A. Cortopassi, F. Duarte, and R. S. Paton, Cation-$\pi$ interactions in protein-ligand binding: Theory and data-mining reveal different roles for lysine and arginine, Chem. Sci. **9**, 2655 (2018).
[53] Q. Lu, D. X. Oh, Y. Lee, Y. Jho, D. S. Hwang, and H. Zeng, Nanomechanics of cation-$\pi$ interactions in aqueous solution, Angew. Chem., Int. Ed. **52**, 3944 (2013).
[54] J. Sunner, K. Nishizawa, and P. Kebarle, Ion-solvent molecule interactions in the gas phase. The potassium ion and benzene, J. Chem. Phys. **85**, 1814 (1981).
[55] D. W. Smith, Ionic hydration enthalpies, J. Chem. Educ. **54**, 540 (1977).
[56] A. Lange, K. Seidel, L. Verdier, S. Luca, and M. Baldus, Analysis of proton-proton transfer dynamics in rotating solids and their use for 3D structure determination, J. Am. Chem. Soc. **125**, 12640 (2003).